Supporting Information for "All-optical sensing of a single-molecule electron spin"

A. O. Sushkov,[†,‡,▽] N. Chisholm,[¶,▽] I. Lovchinsky,[†,▽] M. Kubo,[‡] P. K. Lo,[§] S. D. Bennett,[†] D. Hunger,[∥] A. Akimov,[⊥] R. L. Walsworth,[†,#,@] H. Park,[*,†,‡,△] and M. D. Lukin[*,†]

Department of Physics, Harvard University, Cambridge, MA 02138, USA, Department of Chemistry and Chemical Biology, Harvard University, Cambridge, MA 02138, USA, School of Engineering and Applied Sciences, Harvard University, Cambridge, MA 02138, USA, Department of Biology and Chemistry, City University of Hong Kong, Tat Chee Avenue, Kowloon, Hong Kong SAR, China, Max-Planck-Institut für Quantenoptik, Garching, D-85748, Germany, Russian Quantum Center, Skolkovo, Moscow Region, 143025 Russia, Harvard-Smithsonian Center for Astrophysics, Cambridge, Massachusetts 02138, USA, Center for Brain Science, Harvard University, Cambridge, Massachusetts 02138, USA, and Broad Institute of MIT and Harvard, 7 Cambridge Center, Cambridge, MA, 02142, USA

E-mail: Hongkun_Park@harvard.edu; lukin@physics.harvard.edu

Materials and Methods

Diamond samples

The samples used in this work were polished, single-crystal electronic grade diamonds grown by chemical vapor deposition (Element Six). The diamonds were {100}-cut, and contained substitutional nitrogen and boron in concentrations less than 5 parts per billion (ppb) and 1 ppb respectively. Prior to implantation, the diamond surface was etched approximately 1 μm, using an Ar-Cl_2 plasma etch (25 sccm Ar, 40 sccm Cl_2, ICP RF 400 W, bias RF 250 W, duration 150 s), followed by an O_2 plasma etch (30 sccm O_2, ICP RF 700 W, bias RF 100 W, duration 150 s). Nitrogen implantation was done by INNOViON Corporation using a $^{15}N^+$ dosage of 10^9 cm^{-2} and an implantation energy of 3 keV, corresponding to a SRIM calculated depth of (5.3 $\pm$ 2.2) nm. The implanted diamonds were annealed in vacuum using the following procedure: (a) 2 hour ramp to 400°C, (b) 4 hours at 400°C, (c) 2 hour ramp to 800°C, (d) 8 hours at 800°C and (e) 4 hour ramp to room temperature. After annealing, the diamonds were cleaned in a 3-acid mixture (equal volumes of concentrated H_2SO_4, concentrated HNO_3, and 1 M $HClO_4$) for two hours under reflux conditions, followed by air annealing for 10 hours at 420°C.

*To whom correspondence should be addressed
†Department of Physics, Harvard University, Cambridge, MA 02138, USA
‡Department of Chemistry and Chemical Biology, Harvard University, Cambridge, MA 02138, USA
¶School of Engineering and Applied Sciences, Harvard University, Cambridge, MA 02138, USA
§Department of Biology and Chemistry, City University of Hong Kong, Tat Chee Avenue, Kowloon, Hong Kong SAR, China
‖Max-Planck-Institut für Quantenoptik, Garching, D-85748, Germany
⊥Russian Quantum Center, Skolkovo, Moscow Region, 143025 Russia
#Harvard-Smithsonian Center for Astrophysics, Cambridge, Massachusetts 02138, USA
@Center for Brain Science, Harvard University, Cambridge, Massachusetts 02138, USA
△Broad Institute of MIT and Harvard, 7 Cambridge Center, Cambridge, MA, 02142, USA
▽These authors contributed equally to this work

Optical setup

We used a home-built scanning confocal microscope to optically address and read out single NV centers. The diamond was placed with NV-side down on top of a No. 0 glass coverslip. The inverted Nikon Plan Fluor 100x oil immersion objective (NA = 1.3) was positioned under the coverslip. Its vertical position is controlled with a piezoelectric scanner (Physik Instrumente P-721 PIFOC) and the lateral position of the laser beam focus was controlled with a closed-loop scanning galvanometer (Thorlabs GVS012). Optical excitation was performed with a 532 nm laser (Information Unlimited, MLLIII532-200-1) modulated with an acousto-optic modulator (Isomet Corporation, 1250C-974) in a double-pass configuration. NV center fluorescence was filtered with a 532 nm notch filter (Semrock, NF03-532E) and a 633 nm long-pass filter (Semorck, LP02-633RU) and collected using an avalanche photodiode (PerkinElmer, SPCM-AQRH-14-FC). The TTL voltage pulses used in our measurements were produced using a 400 MHz PulseBlasterESR-PRO pulse generator from Spincore Technologies.

Sample preparation

Diamond surface cleaning procedure

The diamond cleaning procedure was optimized to minimize background fluorescence and to ensure that the surface was terminated with carboxyl groups. The samples were cleaned in a 3-acid mixture (equal volumes of concentrated H_2SO_4, concentrated HNO_3, and 1 M $HClO_4$) for 4 hours under reflux conditions, followed by concentrated ultrapure (99.999%) HNO_3 at 90°C for 1 hour, 1.0 M of NaOH at 90°C for one hour and 1.0 M of HCl at 90°C for one hour. The diamonds were washed with ultrapure water after each step.

Gd^{3+}-molecule attachment procedure

Gd^{3+} molecules were synthesized and purified using methods discussed in.[1] To activate the surface carboxyl groups, the diamonds were treated in a solution of 1-ethyl-3-(3-dimethylaminopropyl)carbo (EDC; 100 μM) and *N*-hydroxysuccinimide (NHS; 100 μM) at room temperature for 12 hours. After rinsing with ultrapure water, the diamonds were placed in a 1 mM Gd^{3+}-molecule solution and reacted at room temperature for 2 hours. The diamonds were then rinsed with ultrapure water. The surface density of attached molecules could be decreased by diluting the Gd-ligand solution.

Gd^{3+}-molecule removal procedure

We repeated the cleaning procedure described above to hydrolyze the peptide bonds and remove the Gd^{3+} molecules from the diamond surface.

Determination of Gd^{3+}-molecule surface density

Atomic force microscopy

We used an Asylum MFP-3D atomic force microscope (AFM) in AC mode to image the surfaces of our diamond samples, in air. The probes (Nanosensors SSM-FMR) had a spike radius of (3 $\pm$ 2) nm and a resonant frequency between 45 and 115 Hz. Samples were mounted onto cover slides using SPI die-cut nonconductive double-sided adhesive discs. The AFM trace and retrace data were averaged together linearly.

A typical AFM height image of a diamond surface after Gd^{3+} molecule attachment is shown in Fig. S1A. We determined the mean separation between the surface molecules to be in the range 20 nm to 25 nm. The radii of the circular features (see Fig. S1C) are consistent with the lateral resolution limit imposed by the AFM tip while the height (see Fig. S1B) is consistent with that expected for single Gd^{3+} molecules, estimated from bond lengths and

angles. The orientation of the molecules on the surface in ambient conditions is unknown, and the variation of orientations likely contributes to the range of AFM spot heights.

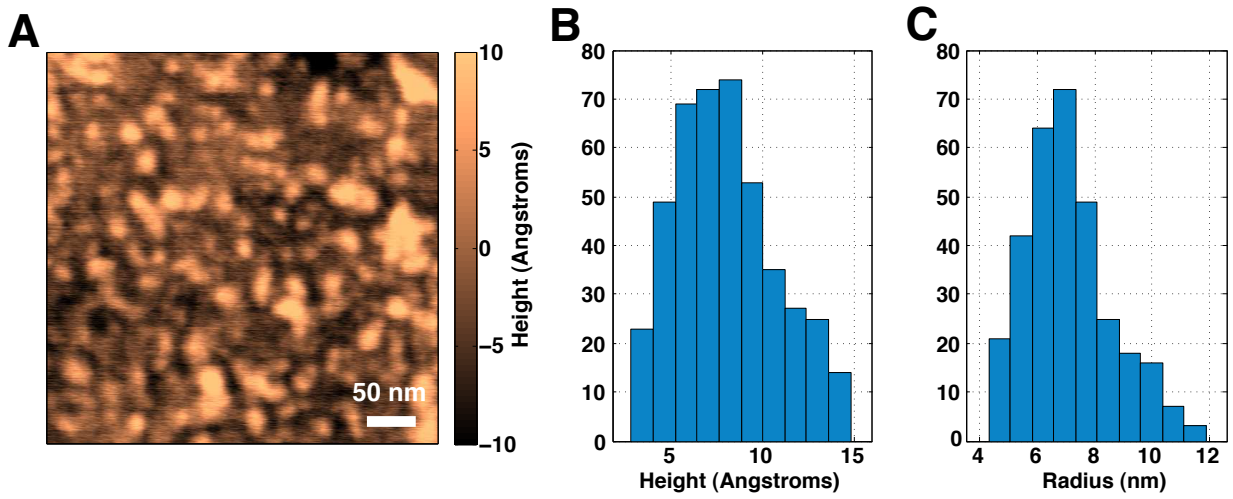


Figure S1: Determination of the size of a single Gd^{3+} molecule. (A) 350 nm × 350 nm AFM height image of a diamond surface with Gd^{3+} molecules attached. (B) Histogram of the heights of the circular features in an larger AFM image, of approximate size 3 μm × 3 μm. The mean height of a single Gd^{3+} molecule is determined to be (8 ± 3) Å. (C) Histogram of the radii of these features. The mean radius of a feature that corresponds to a single Gd^{3+} molecule is found to be (7 ± 2) nm.

To confirm that these surface features are indeed single Gd^{3+} molecules, we attached to each molecule a single Cy3 fluorescent dye, attached the resulting Cy3-Gd^{3+} molecule to the diamond surface, and correlated the Cy3 fluorescence rate observed in our confocal microscope with the surface density observed in the AFM images. We calibrated the fluorescence rate of a single Cy3-Gd^{3+} molecule by attaching an optically resolvable concentration (achieved by diluting the stock ligand solution) of these molecules to the diamond surface and monitoring the fluorescence rate in the 542 - 633 nm band, filtering out fluorescence from NV centres (Fig. S2A). A typical fluorescence time trace of a single Cy3-Gd^{3+} molecule under CW 532 nm illumination (2 μW) is shown in Fig. S2B and displays a photo-bleaching pattern characteristic of a single-molecule emitter. We detected a mean fluorescence rate of 1200 photons/second from a single fluorescent Cy3-Gd^{3+} molecule. At high concentration, the surface molecules were no longer optically-resolvable (Fig. S2C) but the fluorescence rate

in a diffraction-limited focal spot suggested a mean surface density in the range $1/(20\ \mathrm{nm})^2$ to $1/(25\ \mathrm{nm})^2$, consistent with that obtained in AFM measurements described above. Finally, inspection of this area of the surface in the AFM revealed circular features with height, radius and density that were in good agreement with those found after attaching Gd^{3+} molecules (see Fig. S2D).

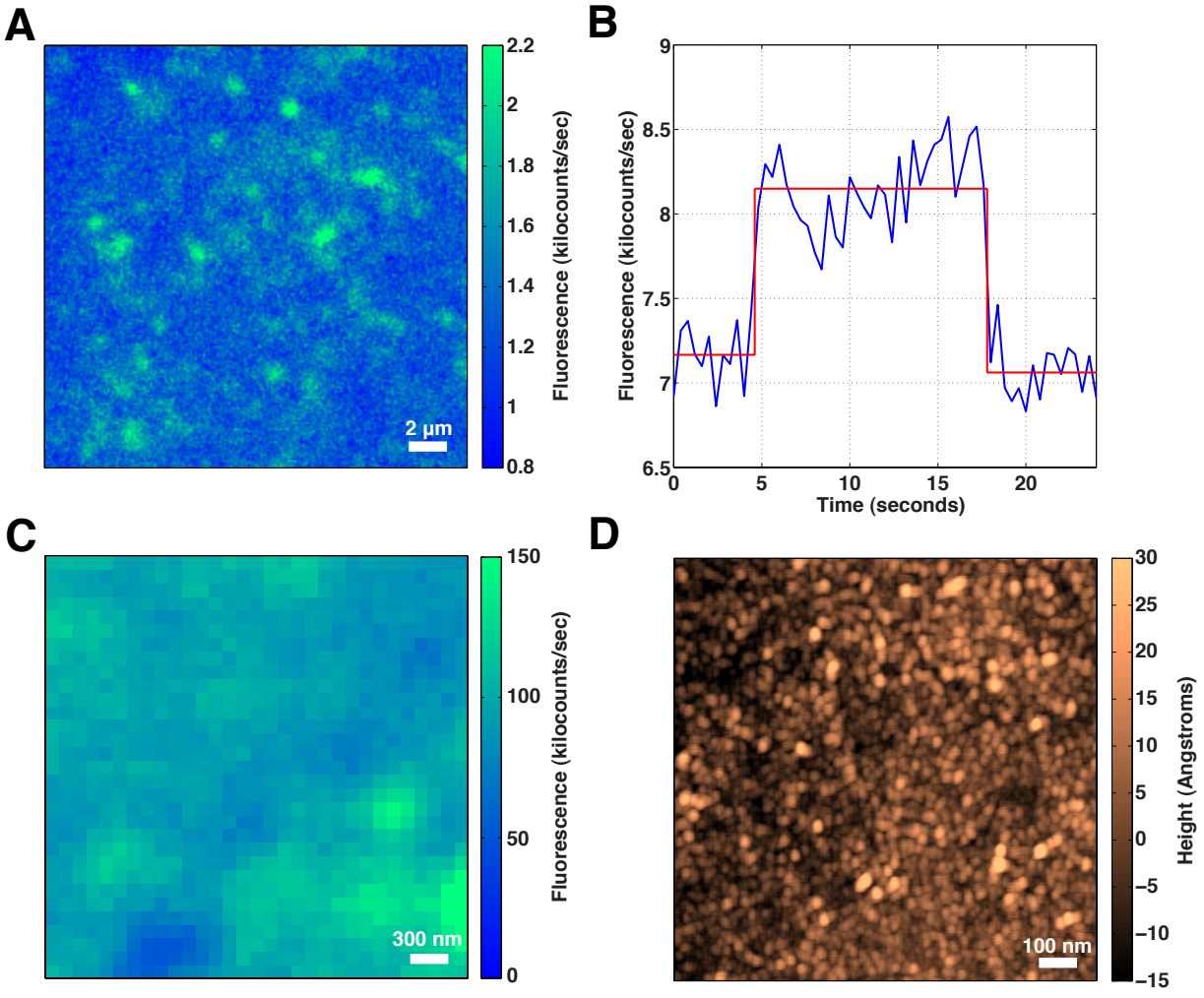


Figure S2: Determination of Gd^{3+} molecule surface density. (A) 20 μm × 20 μm fluorescence image of single Cy3-ligand molecules. (B) Photobleaching of a single Cy3-ligand molecule under CW 532 nm laser illumination (2 μW). (C) 3 μm × 3 μm fluorescence image of a diamond surface saturated with Cy3-ligand molecules. (D) 1 μm × 1 μm AFM height image of the same diamond surface as in Fig. S2C.

We conclude that the observed features are indeed single Gd^{3+} molecules. We note

that the surface concentration could be controlled by diluting the ligand solution and our attachment procedure resulted in a uniform distribution of molecules, with little aggregation.

These molecules are attached to the diamond via the surface carboxylic groups. Some surface carboxylic groups may be chemically unreactive (due, for example, to steric hindrance by neighboring surface groups, or other surface structure considerations[2–4]) and do not attach the Gd^{3+} molecules. From our measurements we conclude that the surface density of the "reactive" carboxylic groups is in the range $1/(20\text{ nm})^2$ to $1/(25\text{ nm})^2$.

Co-localization procedure

AFM drift correction

It took on the order of an hour to acquire each of the AFM scans used in our measurements. During that time, the AFM image underwent lateral drift, with typical magnitude of 10 nm per hour to 100 nm per hour. This introduced a shift in the relative positions of the features at the top of an AFM image, taken near the beginning of a scan, relative to the features at the bottom of an AFM image, taken near the end of the scan. In order to correct for the drift, we always acquired two consecutive AFM scans of the same area of the diamond surface, and, using numerical image processing, extracted the magnitude of the drift. We then corrected each of the two images for this drift, and averaged them together.

Co-localization steps

We determined the separation between an NV centre and the nearest Gd^{3+} molecule in a three-step co-localization procedure. First, the diamond surface was coated (via electrostatic attachment) with an optically resolvable density of 100 nm-diameter gold nanoparticles. These nanoparticles fluoresce in the same spectral region as the NV centres, and thus could be observed simultaneously with NV centers in our scanning confocal microscope. We compiled a map of the surface positions of these nanoparticles, together with a map of the NV centers

in the same region (Fig. 2A). In the second step, the surface topography of this diamond was measured using the AFM (Fig. 2B). The gold nanoparticles could be clearly seen, together with a number of topographic features (pits and scratches) in the diamond surface, thus enabling us to compile a map of the positions of these surface features relative to the nanoparticles. Finally, after cleaning off the nanoparticles, we attached Gd^{3+} molecules to the diamond surface, and the diamond surface topography was measured using the AFM, yielding a map of the positions of the Gd^{3+} molecules in relation to the surface features. We used these three maps to deduce the positions of the Gd^{3+} molecules relative to the NV centers (Fig. 2C).

Co-localization uncertainty

The uncertainty in the position of an NV center relative to the Gd^{3+} molecules on the diamond surface was estimated by combining the uncertainties in each of the co-localization steps in quadrature. The dominant uncertainty, on the order of 10 nm, arose when matching the fluorescence and AFM maps of the nanoparticle positions. We used between 9 and 15 nanoparticles in this step. Their coordinates were extracted from Gaussian fits to the fluorescent spots in the confocal scan, and from spherical-dome fits to the corresponding features in the AFM scan. We deduced the position of the NV center in the AFM image by finding the transformation (scaling + rotation) that most accurately maps the fluorescence-scan coordinates of the nanoparticles to their coordinates in the AFM image and applying this transformation to the NV center fluorescence-scan coordinates. In order to estimate the associated uncertainty in the NV center AFM-scan coordinates, we ran Monte Carlo simulations that shifted each of the nanoparticles by a randomly-oriented normally distributed vector with a standard deviation equal to the mean distance between the transformed fluorescence-scan coordinates and the AFM-scan coordinates of the nanospheres, and then calculated the resultant NV center AFM positions. We set the uncertainty in the NV center AFM coordinates to be equal to the standard deviation of the resulting Gaussian distribution of the NV

positions, see Fig. S3. A similar procedure was implemented to estimate the uncertainties arising from the other two co-localization steps. The resulting total uncertainty was typically 15 nm.

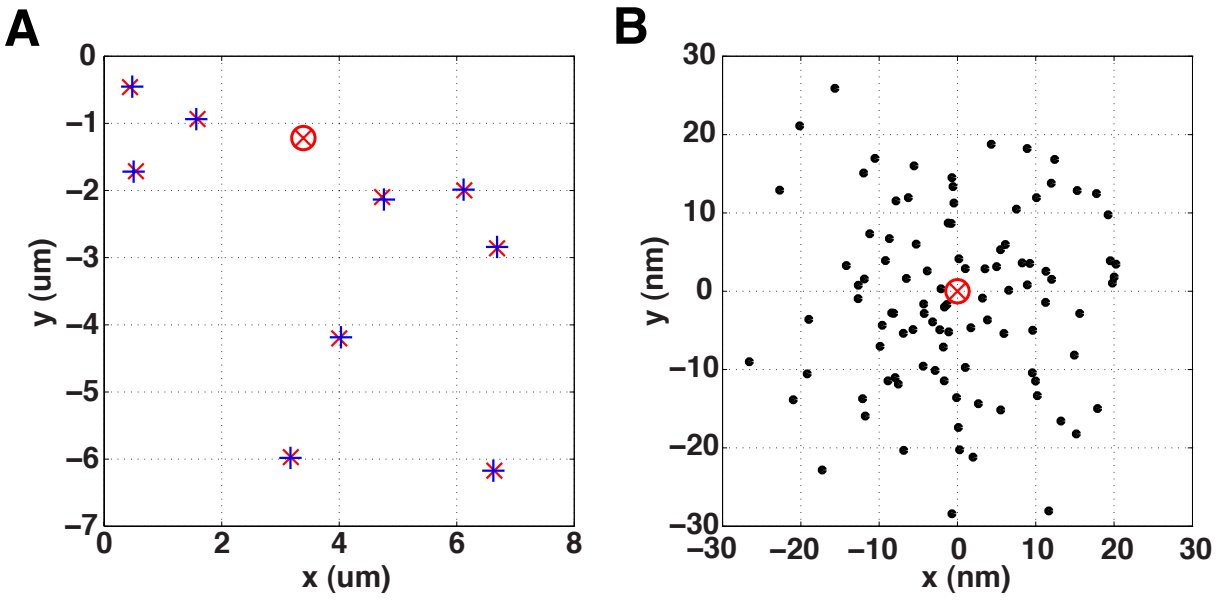


Figure S3: Determination of co-localization uncertainty. (A) The transformed fluorescence image coordinates of an NV center (red circle with a cross) and the gold nanoparticles (all the other red crosses) overlayed on the AFM image coordinates of the same gold nanoparticles (blue crosses). (B) Monte Carlo simulation used to determine the error on the NV center position in Fig. S3A. The red circle with a cross shows the most probable position of the NV center (normalized to the origin) while the blue dots show the distribution of possible positions that arise from the imperfect overlap of the fluorescence and AFM coordinates in Fig. S3A. We take the standard deviation of the distribution of these positions to be the co-localization uncertainty. For the NV center shown this is approximately 10 nm, and the average value for all the NV centers is 15 nm.

Derivation of $\Gamma_{induced}$

We describe an NV center interacting with a bath of Gd^{3+} molecules by the Hamiltonian ($\hbar = 1$)

$$H = \frac{\Delta}{2}\sigma_z + \frac{1}{2}g\mu_B \left[B_x(t)\sigma_x + B_y(t)\sigma_y\right] \tag{1}$$

where $\Delta \approx 2.87$ GHz is the zero-field splitting of the NV center, $g \approx 2$ is the electron g-factor, μ_B is the Bohr magneton, $\sigma_{x,y,z}$ are the Pauli spin operators, and $B_{x,y}(t)$ are the transverse components of the fluctuating magnetic field created at the NV center by the proximal Gd^{3+} spins. Here we consider the dynamics within the two-level subspace spanned by the states $|0\rangle$ and $|1\rangle$ of the NV center ground state triplet and treat $B(t)$ as a classical variable. The z-axis is chosen to be along the symmetry axis of the NV center and we ignore the term $\frac{1}{2}g\mu_B B_z(t)\sigma_z$ since its effect is suppressed by the large zero-field splitting. We take the state of the effective two-level system to be

$$|\psi(t)\rangle = \alpha(t)|0\rangle + \beta(t)|1\rangle. \tag{2}$$

For an NV center initially prepared in the $|0\rangle$ state, first-order time-dependent perturbation theory in the interaction pictures gives[5]

$$\beta(t) = \frac{-i}{2}g\mu_B \int_0^t d\tau[\langle 1|\sigma_x(\tau)|0\rangle B_x(\tau) + \langle 1|\sigma_y(\tau)|0\rangle B_y(\tau)] = \frac{-i}{2}g\mu_B \int_0^t d\tau e^{i\Delta\tau} B_\perp(\tau) \tag{3}$$

for the amplitude of state $|1\rangle$. Here $B_\perp$ is the transverse component of the fluctuating magnetic field. Averaging over the classical variable $B_\perp(\tau)$, the transition probability is given by

$$P_1(t) = |\beta(t)|^2 = \frac{1}{4}g^2\mu_B^2 \int_0^t d\tau_1 \int_0^t d\tau_2 e^{-i\Delta(\tau_1-\tau_2)}\langle B_\perp(\tau_1)B_\perp(\tau_2)\rangle. \tag{4}$$

Using the Wiener-Khinchin theorem, the transition rate becomes

$$\Gamma_{0\to1} = \frac{1}{4}g^2\mu_B^2 S_B(-\Delta), \tag{5}$$

where $S_B(-\Delta)$ is the power spectral density of $B_\perp(\tau)$. Similarly, if we start with the NV center in state $|1\rangle$, the transition rate is given by

$$\Gamma_{1\to0} = \frac{1}{4}g^2\mu_B^2 S_B(\Delta) \tag{6}$$

Treating the fluctuating field as a classical variable imposes the condition that $\langle B_\perp(\tau)B_\perp(0)\rangle$ is real and thus $\Gamma_{1\to 0} = \Gamma_{0\to 1} = \Gamma$. For the specific case of the NV center interacting with a fluctuating Gd^{3+} spin, we assume a telegraph noise spectrum given by

$$S_B(\Delta) = \frac{2\langle B_\perp^2\rangle\gamma}{\gamma^2 + \Delta^2} \tag{7}$$

where $\langle B_\perp^2\rangle$ is the time-averaged magnetic field component, perpendicular to the NV axis, produced at the NV center by the Gd^{3+} spin and $\gamma = 1/T_1^{Gd}$ is the characteristic spectral width (see Fig. 3A of the main text) given by the Gd^{3+} relaxation rate.

To calculate the induced relaxation rate in our experiment we must account for the 3-level structure of the NV center and consider the transition rates between levels $|0\rangle$ and $|-1\rangle$ of the ground state manifold. Because our measurements of the relaxation rates are done in earth magnetic field, levels $|1\rangle$ and $|-1\rangle$ are approximately degenerate and we assume that

$$\Gamma_{0\to -1} \approx \Gamma_{0\to 1} = \Gamma. \tag{8}$$

Accounting for the 3-level structure, the $|0\rangle$ state population evolves in time according to

$$P_0(t) = \frac{1}{3} + \frac{2}{3}e^{-3\Gamma t} = \frac{1}{3} + \frac{2}{3}e^{-\Gamma_{induced}t} \tag{9}$$

where the effective induced relaxation rate is $\Gamma_{induced} = 3\Gamma$.

A single fluctuating Gd^{3+} magnetic dipole moment μ a distance r away from the NV center creates the magnetic field $\langle B_\perp^2\rangle = 4\mu^2/3r^6$. For a Gd^{3+} ion with spin $S = 7/2$, the dipole moment is $\mu = g\mu_B\sqrt{S(S+1)}$.

Combining the above expressions, we obtain the scaling of the NV-center sublevel population relaxation rate induced by a single fluctuating Gd^{3+} ion a distance r away:

$$\Gamma_{induced} = 2\frac{S(S+1)g^4\mu_B^4}{r^6}\frac{\gamma}{\gamma^2 + \Delta^2}. \tag{10}$$

The NV-center sublevel population relaxation rate induced by other paramagnetic species (such as other lanthanide ions) can also be calculated using this expression.

Co-localization Simulation

The Monte-Carlo simulations of the experiment, shown in Fig. 4, were performed as follows. For a random distribution of Gd^{3+} molecules on the diamond surface, the separation between the NV center and the proximal Gd^{3+} molecule was computed, together with the induced NV center relaxation rate. The mean spacing between Gd^{3+} molecules was taken to be 20 nm, to be consistent with the AFM measurements, and the AFM co-localization uncertainty was taken to be 15 nm. The Gd^{3+} electron-spin relaxation rate has been measured in a number of MRI contrast agents,[6] and depends on several factors, such as the local crystal field environment of the Gd^{3+} ion, and the rotational correlation time for solution-phase measurements. Given the range of values quoted in Ref.,[6] this relaxation rate in our experiments is likely to be between 1 and 100 GHz . For the Monte-Carlo simulations we took a value of 10 GHz, which produced the best agreement between the simulation and the data points, as measured by the Kolmogorov-Smirnov Z-statistic test (see below). The simulations contain 10^9 realizations of the experiment. The color scale in Fig. 4 (inset) shows the probability density of obtaining a particular NV center relaxation rate for a given measured separation between the NV center and the proximal Gd^{3+} molecule.

In order to quantify the agreement between the experimental data points and the expected Gd^{3+}-induced NV center relaxation, we calculated reduced chi-squared statistic for the experimental data and the model presented in SI section V: $\chi_r^2 = 0.8$. The agreement between the data points and the Monte-Carlo simulations is hard to quantify rigorously. A commonly used nonparametric technique is the Kolmogorov-Smirnov test, which quantifies the discrepancy between two statistical distributions.[7] Whereas this test is not distribution-independent for multivariate datasets, it is still a useful measure of the goodness-of-fit.[8] The

value of the two-variable Kolmogorov-Smirnov Z-statistic for the data shown in Fig. 4 (inset) is 1.1, which indicates that the data points are consistent with the simulated distribution. The agreement deteriorated when the simulation was done for other values of NV depth, Gd^{3+} relaxation rate, Gd^{3+} molecule spacing, and co-localization uncertainty. We note that the average NV center depth has the largest effect on the simulation results at small radial separations between the NV center and the Gd^{3+} position ($\lesssim 10$ nm).

Detecting Gd^{3+}-molecules by measuring NV-center relaxation

Range of parameters consistent with experimental data

The binned experimental data presented in Fig. 4 of the main text were consistent with a range of parameters (average NV-center depth, Gd^{3+} relaxation rate, and Gd^{3+} molecule surface concentration). These parameters were strongly constrained by the experimental data in the inset in Fig. 4. However, we can argue that the NV-center interacts, on average, with a single Gd^{3+} molecule, based solely on the binned data presented in Fig. 4. For each NV-center depth, Monte-Carlo simulations were performed to determine which values of the Gd^{3+} relaxation rate and surface concentration resulted in the best least-squares fit to the data shown in Fig. 4. These best-fit values are shown as blue points in Fig. S4.

For NV depths greater than approximately 8 nm, all sets of parameters resulted in chi-squared values greater 5 and are therefore inconsistent with the experimental data. NV-center depths less than 4 nm required a Gd^{3+} relaxation rate above 1 THz, well outside the range of values for this rate found in literature. We note that every suitable combination of parameters (every point on the plot) corresponds to a regime where the induced relaxation

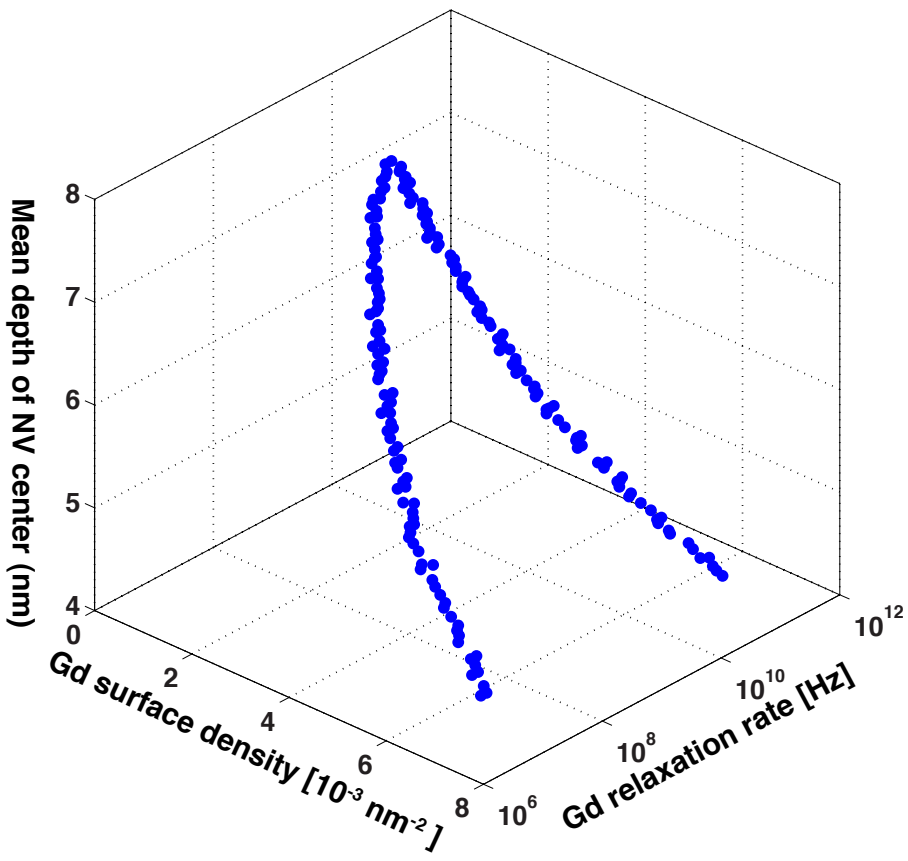


Figure S4: The range of experimental parameters that are consistent with the data. The points show parameter combinations that are consistent with the measured distribution of Gd^{3+}-induced NV-center relaxation rates shown in Fig. 4. All the parameter combinations shown by the points result in $\chi_r^2 < 0.7$.

rate of the NV center is caused by interaction with a single Gd^{3+} spin (the NV center depth is smaller than the mean spacing between the Gd^{3+} molecules).

Experimental Data Uncertainty Analysis

For the binned experimental data shown in Fig. 4, the uncertainties were determined by adding in quadrature the uncertainties resulting from the experimental fitting errors and the bin sampling uncertainties. Each of the 85 measurements (see Fig. 3C) was fit with an exponential decay model, yielding the most likely relaxation rate and a one sigma error bar. These errors allow us to determine the probability that a particular measurement lies

in a particular histogram bin. We considered all possible ways the 85 measurements can be distributed among the five bins and assign probability values to each distribution. This procedure yielded the most likely number of measurements in each bin and the associated one sigma error bar. Additionally, the probability of getting a particular number of measurements in any bin was related to the stochastic distribution of Gd^{3+} molecules on the diamond surface and was binomially distributed. In particular, given a total of N measurements of the relaxation rate, a bin containing n points would have an associated variance given by $n(1 - n/N)$.

Photon shot noise-limited detection sensitivity

A possible paramagnetic molecule detection strategy would be to monitor NV-center fluorescence after optical pumping into the $m_s = 0$ sublevel and a relaxation-in-the-dark period of approximately 2 ms, chosen to be approximately equal to the NV-center intrinsic T_1 time, which we assume to be 5 ms. The photon count rate from a single NV center is typically 5×10^4 s^{-1}. With the 300 ns-long APD photon acquisition window, in such an experiment we can detect approximately 8 photons per second. Given the 30% contrast between the "bright" $m_s = 0$ state, and the "dark" $m_s = \pm 1$ states, a 300 Hz change in NV relaxation rate (which corresponds to detecting a single Gd^{3+} molecule spin at a distance of 10 nm) would result in a photon "signal" of approximately $0.06N_p$, while the "noise" is approximately $\sqrt{N_p}$, where N_p is the detected number of photons. In order to detect this change in NV-center relaxation rate at 3σ confidence level, we need $N_p \approx 2500$ detected photons, which takes approximately five minutes of averaging.

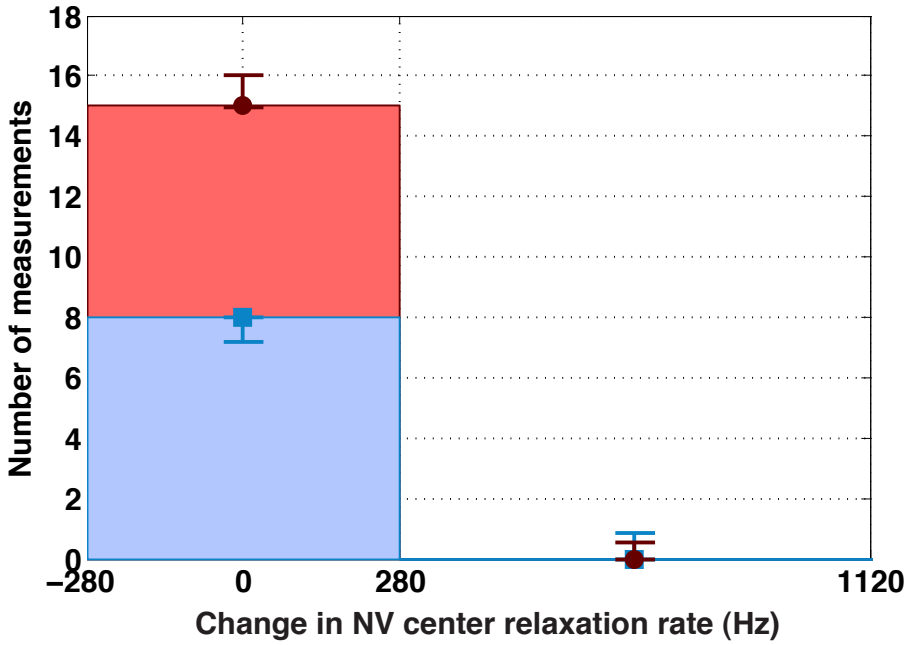


Figure S5: Control experiments with bare ligand and La^{3+} molecules. Experimental results of 16 NV center relaxation rate measurements with bare ligand molecules covalently attached to the diamond surface (red) and 8 NV center relaxation rate measurements with La^{3+} molecules covalently attached to the diamond surface (blue). Within statistical error, the results are consistent with $\Gamma_{induced} = 0$.

Control experiments with La^{3+} containing molecules and bare ligand molecules

In order to demonstrate that the surface chemistry had negligible effect on the relaxation rate of the NV center, we attached bare ligand molecules to the diamond surface. We used the same procedure as for the Gd^{3+} molecules,[1] except in this case we never included gadolinium into the 1 mM solution of ligand molecules. After attaching the bare ligand molecules to the diamond surface, it was clear that no significant increase in relaxation rate was observed for the 16 relaxation measurements taken, as expected (Figure S5). Additionally, we attached La^{3+}-containing molecules to the surface of the diamond. We created La^{3+}-containing molecules in the same way we made Gd^{3+} molecules,[1] but instead replaced Gd^{3+} with La^{3+} to create a 1 mM solution of La^{3+}-containing molecules. La^{3+} is chemically

identical to Gd^{3+}, but it has no unpaired electron spins and thus we expect to see no enhanced relaxation rate. Indeed, we observed no enhanced relaxation rate for the 8 NV center relaxation measurements taken (Figure S5).

References

(1) Henig, J.; Mamedov, I.; Fouskova, P.; Tóth, E.; Logothetis, N. K.; Angelovski, G.; Mayer, H. A. *Inorg. Chem.* **2011**, *50*, 6472–81.

(2) Pehrsson, P. E.; Mercer, T. W. *Surf. Sci.* **2000**, *460*, 74–90.

(3) Strobel, P.; Ristein, J.; Ley, L. *Diamond Relat. Mater.* **2008**, *17*, 1362–1366.

(4) Masel, R. I. *Principles of adsorption and reaction on solid surfaces*; Wiley, New York, 1996.

(5) Clerk, A. A.; Devoret, M. H.; Girvin, S. M.; Marquardt, F.; Schoelkopf, R. J. *Rev. Mod. Phys.* **2010**, *82*, 1155–1208.

(6) Kim, H. K.; Lee, G. H.; Kim, T. J.; Chang, Y. *Bull. Kor. Chem. Soc.* **2009**, *30*, 849.

(7) Feigelson, E. D.; Babu, G. J. *Modern Statistical Methods for Astronomy: With R Applications*; Cambridge University Press, 2012; Vol. 2; p 476.

(8) Peacock, J. *Mon. Not. R. Astron. Soc.* **1983**, *202*, 615–627.